The Role of Lattice Misfit on Heterogeneous Nucleation of Pure Aluminum

L. WANG, L. YANG, D. ZHANG, M. XIA, Y. WANG, and J.G. LI

α-Alumina (Al_2O_3) single crystals with different termination planes were used as heterogeneous nucleation substrates for liquid aluminum to varying lattice misfits at the interface between substrate and newly nucleated aluminum grain. Undercooling during the nucleation process was measured for interface configurations with varied lattice misfit, while the solidified Al/Al_2O_3 interfaces were directly observed by high-resolution transmission electron microscopy (HRTEM). Based on experimental results, the effect of lattice misfit on nucleation behavior was systematically investigated following previous misfit-interfacial energy models, with clarification being made by the undercooling measurement and HRTEM observations of the interfaces in the Al/Al_2O_3 system. When the misfit is smaller than 13 pct, both experimental results and theoretical analysis show that the currently existing models through modification and incorporating energy calculation can be used to fit the detected undercooling of investigated system. Beyond 13 pct, a new hypothesis was developed to accommodate lattice misfit with stacking faults such as microtwins according to the HRTEM analysis. The interfacial energy is then replaced by the stacking fault energy accumulated in the strained area. It is shown that the lattice misfit plays an important role in determining the heterogeneous nucleation of liquid aluminum. The nucleation undercooling is then able to be predicted by the theoretically calculated interfacial energy using the integrated models developed in the work. The prediction results were also verified by the HRTEM analysis on the nucleation interface of the Al/Al_2O_3 systems and detected undercooling on corresponding systems.

DOI: 10.1007/s11661-016-3691-4

I. INTRODUCTION

To understand the solidification behavior of liquid metal, classical nucleation theory (CNT) is formulated with the interfacial energy and volumetric free energy changes of the nucleus formation,[1] where contact angle θ acts as an important factor determining the nucleation potency of a specific heterogeneous substrate. However, for the nucleation on a potential catalyzer (potent substrate), which happens in most of natural nucleation systems, the contact angle is normally very small (close to 0°), and it is hard to form a spherical-cap nucleus.[2] Analyses carried out by X-ray scattering method, atomistic simulation, and in situ transmission electron microscopy (TEM) at high temperature,[3–6] showed that the order of atoms in the liquid increases gradually toward the solid–liquid interface, which is distinguished from the spherical-cap assumption in CNT. Thus, in the case of most natural nucleation systems, the interfacial energy itself, rather than contact angle, becomes a direct criterion for nucleation potency of the substrate.[2,3,7–9]

The interfacial energy is hard to be measured in practice. Turnbull and Vonnegut[10] suggested that the interfacial energy could be predicted by lattice misfit between newly nucleated phase and substrate when lattice misfit f is smaller than 5 pct. That is the first report about the effect of lattice misfit on heterogeneous nucleation of metals based on theoretical analysis and statistics experimental results. Although the energy barrier for the heterogeneous nucleation is induced by the rearrangement of liquid structure toward solid, to overcome the lattice configuration difference between solid-like liquid clusters and substrates is the major energy consumption for a distinct heterogeneous nucleation system. The previous study on the relationship between lattice misfit and interfacial energy was mainly focused on small lattice misfit systems. For example, Frank and van der Merwe[11] pointed out that the interfacial energy is related to lattice misfit for bicrystal when lattice misfit is less than about 4 pct, where elastic distortion strain occurs in the nucleated phase to release the small lattice misfit. For a larger misfit system where edge dislocations will form in a short distance, Matthews *et al.*[12,13] proposed a natural lattice model defining the relationship between interfacial energy and lattice misfit when f is greater than 3.4-4 pct. If misfit is enlarged further into a poor fit system, the interface will match with integral multiple planes by a coincidence

L. WANG, Ph.D. Student, D. ZHANG, Graduate Student, M. XIA, Associate Professor, and J.G. LI, Professor, are with the School of Materials Science and Engineering, Shanghai Jiao Tong University, Shanghai 200240, China. Contact e-mail: mingxu.xia@sjtu.edu.cn L. YANG, Lecturer, is with the School of Materials and Engineering, Jiangsu University of Technology, Changzhou 213001, China. Y. WANG, Researcher, is with the BCAST, Brunel University London, Uxbridge UB8 3PH, UK.

Manuscript submitted March 8, 2016.
Article published online August 10, 2016

lattice model.[14] Vook and Horng[15] observed these coincidence dislocations with a relatively large lattice misfit about 13 pct between Ag and Cu, with the spacing of the coincidence dislocations at least an order of magnitude larger than that of edge dislocations predicted by the natural lattice model theory.

The previous experimental results and related theoretical models described well the relation between interfacial energy and lattice misfit when the misfit is small. However, an effective theoretical model for calculation of the interfacial energy is absent for a system with large misfit, the coincidence lattice misfit system for instance. Besides, the current models are working for different alloys and substrates with discrete lattice misfit range. Most of the research on interfacial energy focus on the system created through vapor deposition or molecular beam epitaxy treatment. So far, there is no direct evidence to demonstrate or to interpret the effect of lattice misfit on heterogeneous nucleation behavior of liquid metal, apart from the original discussions on the relationship between misfit and undercooling[10,16] or initial precipitation and undercooling.[17,18] It is also believed that heterogeneous nucleation might be unpractical when misfit f is greater than 14.4 pct. Furthermore, the discussion in the previous studies was generally based on theoretical analysis without any direct observation on such interfacial lattice structure.

In order to clarify the relationship between heterogeneous nucleation behavior of liquid and lattice misfit at interface in a real alloy system, especially in an extended range of lattice misfit, a liquid Al/single crystal Al_2O_3 system was designed to demonstrate an undercontrolled heterogeneous nucleation with various lattice misfits in a common solidification process. The undercooling and interface configuration of the couple were measured to examine the relationship between lattice misfit and nucleation behavior. Interfacial energy of the system for different couples was calculated using the integrated models based on the previous models and the direct observed results obtained through high-resolution transmission electron microscopy (HRTEM). The validity of the results was examined by measured undercooling of the couples.

II. EXPERIMENTAL

A. *Materials*

High-purity aluminum (>99.999 pct) and Al_2O_3 single crystals were used to form Al/Al_2O_3 couple in the study. Different crystallographic termination planes, such as $(11\bar{2}0)$ and $(10\bar{1}0)$ planes, of the oxide single crystal were cut from commercial sapphire with the orientation $\pm 0.5°$, to vary the lattice misfit with aluminum. The dimension of single crystal plates was $5 \times 5 \times 0.5$ mm, and their surface roughness was less than 0.5 nm. The high-purity Al was used to ensure the nucleation of Al with minimum intrinsic heterogeneous nuclei. The weight of Al specimens was about 0.02 g. Every Al specimen was further purified through melt flux treatment before experiment.

B. *Undercooling Measurement*

The undercooling during heterogeneous nucleation of Al on the single crystal Al_2O_3 substrates was precisely recorded using a pyrometer with an accuracy of ± 1 K (°C). A detailed description of the setup for the undercooling measurement can be referred in Reference 19. Before experiment, the single crystal Al_2O_3 substrates were thoroughly cleaned in acetone for 3 minutes with an ultrasonic cleanser and then placed on a gas cooling platform in a high vacuum chamber (the pressure was 2×10^{-4} Pa). An aluminum sample was placed on such an Al_2O_3 substrate and Al/Al_2O_3 couple was heated up to 1300 K (1027 °C) by a laser beam with a heating rate of 20 K (°C)/s. The sample was holding at the temperature for 3 minutes before the laser beam was switched off, and then cooled down at a controlled cooling rate 20 K (°C)/s under a flowing argon atmosphere. The cooling curve of Al droplet on Al_2O_3 substrate was recorded, from which the undercooling was defined as the temperature difference between the recalescence temperature and nucleation temperature. The measurement was made in multiple experimental runs in order to ensure the reliability of the experimental results.

C. *Lattice Misfit of Al/Al_2O_3 Couples*

Lattice misfit can be obtained through Turnbull's one-dimension model[10] where only the low index directions on low index planes of a nucleation system will be calculated. Bramfitt[16] extended this model into a two-dimension model where 3 directions will be concerned in low index planes of a system. Apart from these two models, edge-to-edge matching model[20–25] based on minimization of the strain energy of the interface and actual atom rows matching[21] was used to predict the orientation relationships and the corresponding habit planes (the interface between the new and parent phases) over a range of lattice misfit less than 10 pct, where the misfit was calculated either at the edge matching direction or at the matching parallel planes for the diffusion-controlled phase transformation couples and epitaxial growth systems. In our system, the nucleation plane was triggered on the selected terminated planes of substrate. The artificially created nucleation interface is part of over the range of the above models. To facilitate the real-matching planes, X-ray diffraction (XRD), carried out by Rigaku Ultima IV X-ray diffractometer with monochromatic CuKα radiation (λ = 0.154060 nm), was employed to determine the matching planes between the solidified Al and Al_2O_3 substrate with various termination planes. The XRD patterns in Figure 1 show that the strongest peak, *i.e.*, the most preferred orientation of the solidified Al varies with the termination planes of the substrate.

Theoretically, the two-dimensional lattice misfit f of two matching planes was calculated based on the following Bramfitt equation[16]:

$$f^{(hkl)_s}_{(hkl)_n} = \sum_{i=1}^{3} \frac{\left| d_{[uvw]^i_s} \cos\theta - d_{[uvw]^i_n} \right|}{3 d_{[uvw]^i_n}} \times 100\,\text{pct}, \qquad [1]$$

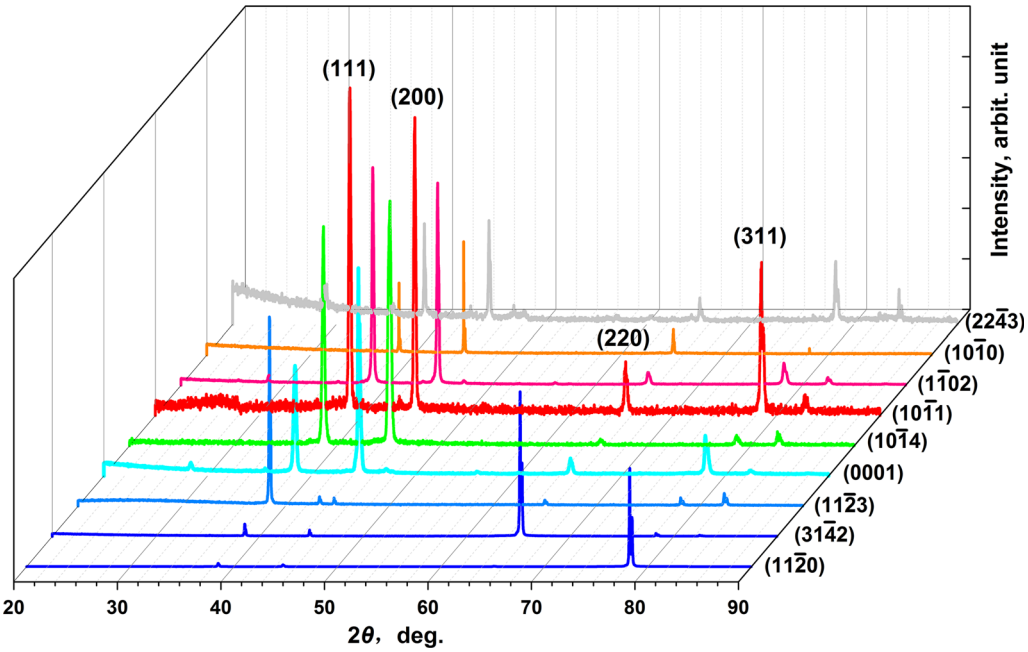

Fig. 1—XRD patterns of Al surface adjacent to Al_2O_3 substrates with (22$\bar{4}$3), (10$\bar{1}$0), (1$\bar{1}$02), (10$\bar{1}$1), (10$\bar{1}$4), (0001), (11$\bar{2}$3), (31$\bar{4}$2), (11$\bar{2}$0) termination planes.

where $d_{[uvw]s}$, $d_{[uvw]n}$ are the interatomic spacings along direction $[uvw]_s$, $[uvw]_n$ and θ is the angle between $[uvw]_s$ and $[uvw]_n$. The subscript s and n stands for substrate and nucleated crystal, respectively. It should be noted that planes of $(hkl)_s$ and $(hkl)_n$ used in this work are not the low index planes as stated in Bramfitt's model. Due to the single crystal feature of the substrate, $(hkl)_s$ in the equation is termination plane of substrate, $[uvw]_s$ is a low index direction in $(hkl)_s$, $(hkl)_n$ is the growth plane of the newly nucleated phase, and $[uvw]_n$ is a low index direction in $(hkl)_n$.

Taking into account the lattice expansion at high temperature, lattice parameter a of Al is 0.412 nm, and a and c of α-Al_2O_3 are 0.478 and 1.306 nm, respectively, when Al solidified on the surface of Al_2O_3.[26–28] A series of theoretical lattice misfits between Al and Al_2O_3 were obtained according to XRD results and are listed in Table I. It is noted that the intensity of (111) and (200) peak is almost close to each other when Al solidified on (10$\bar{1}$1) Al_2O_3 substrate and the theoretical lattice misfits of (111) Al/(10$\bar{1}$1) Al_2O_3 and (200) Al/(10$\bar{1}$1) Al_2O_3 are nearly the same. A smaller lattice misfit of (200) Al/(10$\bar{1}$1) Al_2O_3 is selected for the further analysis. So does the misfit of (111) Al/(10$\bar{1}$4) Al_2O_3.

D. *TEM and HRTEM*

In order to further investigate the crystal orientation and in-plane textures of nucleated crystal Al at the Al/Al_2O_3 interface, thin cross-sectional foil specimens were prepared by mechanical grinding, and then extracted and thinned by focus ion beam (FIB) using FEI Helios 600i system at 30 kV for TEM and HRTEM examinations. TEM and HRTEM were carried out using a Tecnai G^2s-Twin microscope operating at 200 kV, with the point resolution 0.24 nm.

III. RESULTS

A. *Nucleation Undercooling of Al/Al_2O_3 Systems*

The measurements of the nucleation undercooling on different termination planes are listed in Table I, together with the theoretically calculated lattice misfit and plotted in Figure 2. It is observed that the undercooling is closely related to the lattice misfit. When $f <$ ~13 pct, the undercooling increases from 3.5 K ± 1.4 K (°C) with f = 7.77 pct to 39.6 K ± 5.4 K (°C) with f = 12.90 pct. As suggested by Bramfitt,[16] the trend of the undercooling can be fitted with a parabolic relationship when the lattice misfit is smaller than 12.49 pct in the study

$$\Delta T = 0.09 \cdot f^2 \qquad [2]$$

where the coefficient of correlation, R^2, of the parabolic relationship is 0.9120. It is found that the undercooling exceeds the predicted value at about 13 pct in our experiments, so do the data of Fe/WC 29 K (°C) with misfit 12.7 pct.[16] Given $f >$ 13 pct, the undercooling sharply increases to 25.2 K ± 2.0 K (°C) where the misfit is 16.36 pct. Then the undercooling decreases slightly to 19.0 K ± 1.3 K (°C) with a misfit increasing to 25.03 pct, with a linear relationship at this range as follows:

$$\Delta T = 37.31 - 0.73 \cdot f \qquad [3]$$

Table I. The Theoretical Lattice Misfits (f) Between Al and Al_2O_3 Single Crystal Substrates and the Corresponding Undercooling Obtained on Different Substrates and its Standard Deviation

No	Matching planes	f (pct)	ΔT (K)	σ (K)
1	(100) Al/(22$\bar{4}$3) Al_2O_3	7.77	3.5	1.4
2	(100) Al/(10$\bar{1}$0) Al_2O_3	9.45	5.8	0.8
3	(111) Al/(1$\bar{1}$02) Al_2O_3	12.49	16.0	2.5
4	(100) Al/(10$\bar{1}$1) Al_2O_3	12.77	32.7	4.9
5	(111) Al/(10$\bar{1}$4) Al_2O_3	12.90	39.6	5.4
6	(100) Al/(0001) Al_2O_3	16.36	25.2	2.0
7	(111) Al/(11$\bar{2}$3) Al_2O_3	17.10	25.1	4.2
8	(110) Al/(31$\bar{4}$2) Al_2O_3	21.42	22.4	2.7
9	(311) Al/(11$\bar{2}$0) Al_2O_3	25.03	19.0	1.3

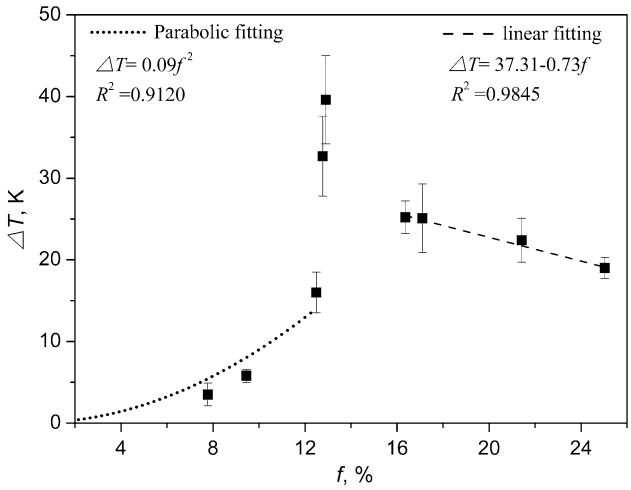

Fig. 2—Nucleation undercooling of Al solidified on different single crystal Al_2O_3 substrates related to theoretical lattice misfit. When $f <$ ~13 pct, the trend of the undercooling follows a parabolic relationship with lattice misfit as $\Delta T = 0.09\, f^2$, while the undercooling exceeds the predicted value at about $f = 13$ pct. After $f > 13$ pct, the undercooling sharply increases to 25.2 ± 2.0 K (°C) where misfit is 16.36 pct and then the undercooling decreases slightly, with a linear relationship at this range as $\Delta T = 37.31\text{-}0.73 \cdot f$.

where the coefficient of correlation, R^2, of the linear relationship is 0.9845. The decrease of undercooling indicates that the nucleation mechanism varies when $f >$ 13 pct.

B. *Characteristics of Al/Al_2O_3 Interfaces*

To further investigate the variation of nucleation behavior, samples solidified on (10$\bar{1}$1), (0001), and (11$\bar{2}$0) planes were examined using TEM and HRTEM, with the lattice misfit f being 12.77, 16.36, and 25.03 pct, respectively. The bright-field TEM images in Figure 3 show that there are two different types of interface. When $f < 13$ pct, a clear and sharp interface was observed as shown in Figure 3(a). When $f > 13$ pct, however, an extra plate phase was found at the Al/Al_2O_3 interface, as marked "A, B" in Figure 3(b) and (c), respectively. Energy dispersive spectrometry (EDS) revealed that the extra phase at the interface was composed of pure Al, as described in a previous study.[19]

1. *Al/Al_2O_3 interface with 12.77 pct misfit*

Figure 4(a) is the inverse fast Fourier transformation (IFFT) image of cross-sectional HRTEM of the sample solidified on (10$\bar{1}$1) plane (f = 12.77 pct), with the Al crystal being viewed along its [001] zone axis. The lattice arrangement of Al_2O_3 and Al is clearly seen in the lower and upper area, respectively, in Figure 4(a). The interface between Al_2O_3 and Al is marked with white dashed line. It is seen that (20$\bar{2}$2) plane of Al_2O_3 is parallel to the interface and the arrangement of (20$\bar{2}$2) is same to that of (10$\bar{1}$1). That is to say the (10$\bar{1}$1) plane is parallel to the interface. Meanwhile, every five (0$\bar{2}$0) planes of Al crystal with d-spacing of 0.198 nm matches with three (10$\bar{1}\bar{2}$) planes of Al_2O_3 substrate with d-spacing of 0.346 nm. The lattice arrangement of Al and Al_2O_3 is marked with yellow and red circles, respectively. The coincidence matching between Al and Al_2O_3 at the interface is schematically illustrated in Figure 4(d). The total distance associated with three lattice rows in the substrate is somewhat smaller than that associated with five lattice rows in the crystal, so that the coincidence structure places the crystal under compressive stress. Figure 4(b) is the FFT pattern of Al/(10$\bar{1}$1)Al_2O_3 HRTEM interface, where the incident beam is aligned along [001] of Al zone axis. At the same time, the Al_2O_3 substrate is viewed along its [1$\bar{2}$10] zone axis. A schematic index of the pattern is shown in Figure 4(c), where the open and filled circles represent Al and Al_2O_3 respectively.

2. *Strained area at the interface with misfit of 16.36 pct*

Figure 5 shows the cross-sectional HRTEM image of the sample solidified on (0001) surface. As shown in Table I, the misfit between the newly nucleated Al and Al_2O_3 (0001) substrate is calculated to be 16.36 pct, if (100) Al matches the (0001) basal plane of Al_2O_3. In Figure 5(a), the incident electron beam is parallel to [1$\bar{1}$00] axis of Al_2O_3, with its (0001) planes being parallel to the interface. The interface is marked with black dashed line. Above Al_2O_3 crystal, the plate contains a few periodic lattice site arranging layers with average spacing of the interlayer parallel to interface about 0.839 nm and the plane spacing along horizontal direction about 0.285 nm. Above the plate, Al crystal with (200) planes grows on the plate in Figure 5(b).

The SAED patterns on the interface between plate/Al_2O_3 and plate/Al both show overlapped spots in

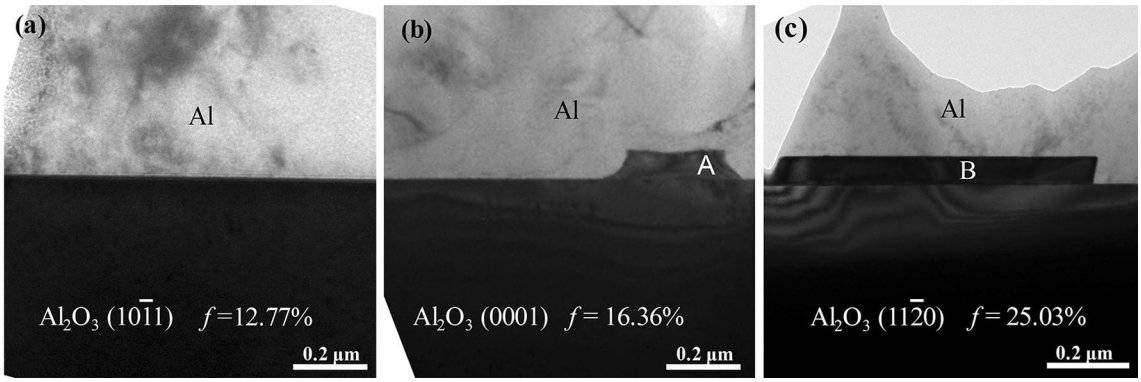

Fig. 3—The cross-sectional TEM bright-field images of (*a*) Al/Al_2O_3 (10$\bar{1}$1) with f = 12.77 pct, (*b*) Al/Al_2O_3 (0001) with f = 16.36 pct, (*c*) Al/Al_2O_3 (11$\bar{2}$0) with f = 25.03 pct. The discontinuous plates were composed of pure Al by examination of energy dispersive spectrometer (EDS)[19] at the interface adjacent to Al_2O_3, as marked "A, B" in (b), (c).

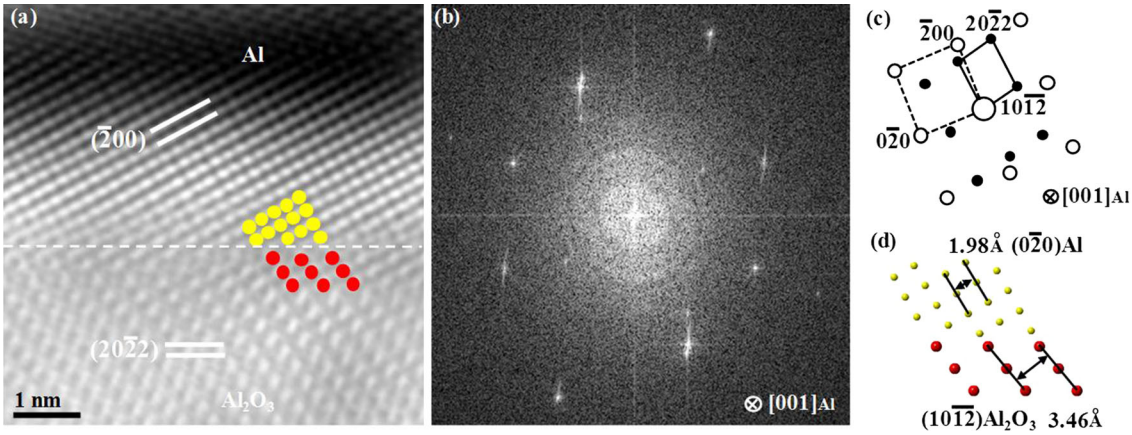

Fig. 4—The inverse fast Fourier transformation (IFFT) (*a*) and FFT (*b*) image of cross-sectional HRTEM of Al/Al_2O_3 (10$\bar{1}$1) interface taken along Al [001] axis. (*c*) Schematic showing the index of the FFT pattern along $[001]_{Al}$ zone axis, where the open and filled circles represent Al and Al_2O_3, respectively. (*d*) Schematic illustrating the coincidence matching between Al and Al_2O_3 at the interface. Every five (0$\bar{2}$0) planes of Al crystal with *d*-spacing of 0.198 nm matches with three (10$\bar{1}$2) planes of Al_2O_3 substrate with *d*-spacing of 0.346 nm. The lattice arrangement of Al and Al_2O_3 is marked with yellow and red circles, respectively.

Figure 5(c) and (d).Through the analysis of the SADPs, there are both three sets of diffraction patterns. In Figure 5(c), one set is hexagonal structure with *d*-spacing of 0.432 and 0.238 nm corresponding to {0003} and {11$\bar{2}$0} planes of Al_2O_3 as indexed with large open circles. The other two sets are characterized by satellite spots shifting about 1/3 distance from the principal reflection spots, with the same *d*-spacing about 0.285 nm corresponding to {110} planes of Al and 0.839 nm without any corresponding plane for Al or Al_2O_3. The spots have typical feature of twins with habit plane (100) and invariant direction [001] as schematically illustrated with filled white and red circles in the pattern. The same principal and satellite spots also occur in Figure 5(d), and the third set is face-centered cubic structure with plane spacing of 0.202 nm and 0.143 nm corresponding to {200} and {220} planes of Al being viewed from its [001] zone axis.

From the above analysis, we found that the interlayer spacing of planes parallel to the interface is just equal to the spacing related to the unidentifiable spots in SADPs and the other spacing corresponds to the {110} planes of Al. Combined our results with the analysis of microtwinned structure reported by Pérez-Sierra,[29] it is believed that the structure is microtwin and there are two or three atomic layers in each twin layer. The layer adjacent to the interface is a little ambiguous possibly due to the disorder stacking sequence, overlapped lattices of the plates, or the presence of strain at the interfaces.

3. *Strained area at the interface with misfit of 25.03 pct*

Similar plates were also observed at the interface in Al/Al_2O_3 (11$\bar{2}$0) system with the incident electron beam parallel to [0001] axis of Al_2O_3, as shown in Figure 6(a). The misfit between newly nucleated Al and Al_2O_3 (11$\bar{2}$0) substrate is calculated to be 25.03 pct, if (311) Al matches (11$\bar{2}$0) the basal plane of Al_2O_3. The interface is marked with white dashed line. It is seen that (11$\bar{2}$0) plane of Al_2O_3 is parallel to the interface. The SADPs on the interface also show overlapped spots in Figure 6(b). Among the spots, a set can be identified as Al_2O_3 in [0001] zone axis as indexed. The other two sets have typical feature of microtwins with habit plane

(100) and invariant direction [001] as schematically illustrated in the pattern. The microtwins have the average spacing of plane parallel to interface which is about 0.845 nm and the other spacing along horizontal direction which is 0.286 nm.

IV. DISCUSSION

Although extensive researches regarding growth of various materials on potent substrates have been performed over the decades, a straightforward demonstration of lattice misfit effect on nucleation behavior is still lacking, without mention of a reasonable explanation for the effectiveness of nucleation substrate. Combining with the experimental results and misfit-interfacial energy models presented here, a hypothesis for the effect of the lattice misfit on the nucleation behavior of liquid Al is given in the following sections.

A. *Misfit-Interfacial Energy Models for Al with Various Misfits*

In this research, different lattice misfits arise when the substrates with different terminating planes were varied for nucleating. The newly nucleated phase may occur with elastic distortion or misfit dislocations in case of a noncoherent interfaces.[11–15]

1. *Nucleation with lattice distortion*

Interfacial energy for the system with small lattice misfit was explained by van der Merwe[30] on the basis of the Peierls–Nabarro's single dislocation model.[31,32] In this model, the total interfacial energy E_{total} per unit area consists of two parts, the strain energy E_s in each half-crystal and the mean energy of misfit E_m due to the sinusoidal force at the interface.[30] Taking into account the growth of crystalline phase,[33] a critical thickness h_{cs} of homogeneous strain layer exists,

$$h_{cs} = \frac{E_s(1-2\upsilon)}{G(1-\upsilon)f^2}, \qquad [4]$$

where bulk modulus G = 16.2 GPa, poison ration υ = 0.369,[34] and f is lattice misfit. The total calculated interfacial energy, the mean energy of misfit, the strain energy per unit area, and the critical thickness of the homogeneous strain layer as a function of lattice misfit for nucleation of Al with distortion are shown in Figure 7 according to Reference 30. It is seen that the upper limit of lattice misfit for pure distortion strain interface is 3.1 pct, where the minimum critical thickness at this point is 0.3 nm, about one atomic layer thick of Al.

2. *Nucleation with natural misfit dislocations*

Natural lattice misfit model (NLM) was proposed by Matthews and his coworkers[12,35,36] to describe the misfit accommodated by dislocations and residual strain. The concerned misfit range is beyond van der Merwe model. The model predicted the interface structure and the critical thickness for the formation of edge dislocations from force balance. People and Bean[13] extended the model from pure edge dislocations to screw types by energy balance. The upper limit of lattice misfits for introducing edge and screw dislocations are 5.8 and 5.4 pct, where the critical thickness values are 0.3 and 0.8 nm, respectively, about one or three atomic layers, the minimum thickness for edge dislocation, and screw dislocation.

However, according to the previous calculation, there is an overlap misfit range where both edge dislocation and screw dislocation are able to be introduced. Actually, the total energy of Al/Al_2O_3 system relaxed by edge dislocation and residual strain is smaller than that of screw dislocation. Given an interfacial energy over the minimum limitation of screw dislocation, the edge dislocations will be easily introduced first and then the rest of energy might be settled by screw dislocations, *i.e.*, a mixed-type dislocation could be introduced. In fact, edge, screw, and mixed-type dislocations[37,38] were all observed at the interface between the epitaxial GaN thin films and sapphire substrate. Thus, it is reasonable to propose the modification of natural lattice model from single-type dislocation toward mixed-type dislocation. For simplification, we assumed that (a) the energy of mixed-type dislocation is dominated by screw dislocation; (b) the minimum thickness for mixed-type dislocations is also fixed by thickness introducing screw dislocations. Then the lattice misfit f for the formation of mixed-type dislocations can be given by

$$f = \sqrt{\left(\frac{1-\nu}{1+\nu}\right)\frac{1}{16\sqrt{2}\pi a_0}\left(\frac{\boldsymbol{b}^2\cos^2\varphi}{h_c}\right)\ln\left(\frac{h_c}{\boldsymbol{b}\cos\varphi}\right)} \qquad [5]$$

where h_c = 0.8 nm, the minimum thickness for screw dislocations, φ is defined as the angle between the Burgers vector and line direction of the dislocation ($0 < \varphi < 65$ deg). Beyond h_c = 0.8 nm, mixed dislocations will be introduced, where misfit is 4.3 pct. The maximum lattice misfit f is 7.8 pct at the angle approach 0. The energy of mixed-type dislocation on Al/Al_2O_3 system for $4.3 < f < 7.8$ pct per unit area can be calculated as

$$E_{md} = E_{ed} + E_{sd} = \frac{G\boldsymbol{b}f\sin^2\varphi}{2\pi(1-\nu)}\left(\ln\frac{0.8\cdot10^{-9}}{\boldsymbol{b}\sin\varphi}+1\right) + \frac{G\boldsymbol{b}^2\cos^2\varphi}{8\pi\sqrt{2}a_0}\ln\left(\frac{0.8\cdot10^{-9}}{\boldsymbol{b}\cos\varphi}\right). \qquad [6]$$

The strain energy E_s per unit area is given by

$$E_s = 2G\left(\frac{1+\nu}{1-\nu}\right)(0.8\cdot10^{-9})f^2 \qquad [7]$$

The calculated total interfacial energy, the energy of dislocation, the strain energy per unit area, and critical thickness for introducing dislocations as a function of natural lattice misfit for nucleation of Al with natural misfit dislocations are plotted in Figure 8.

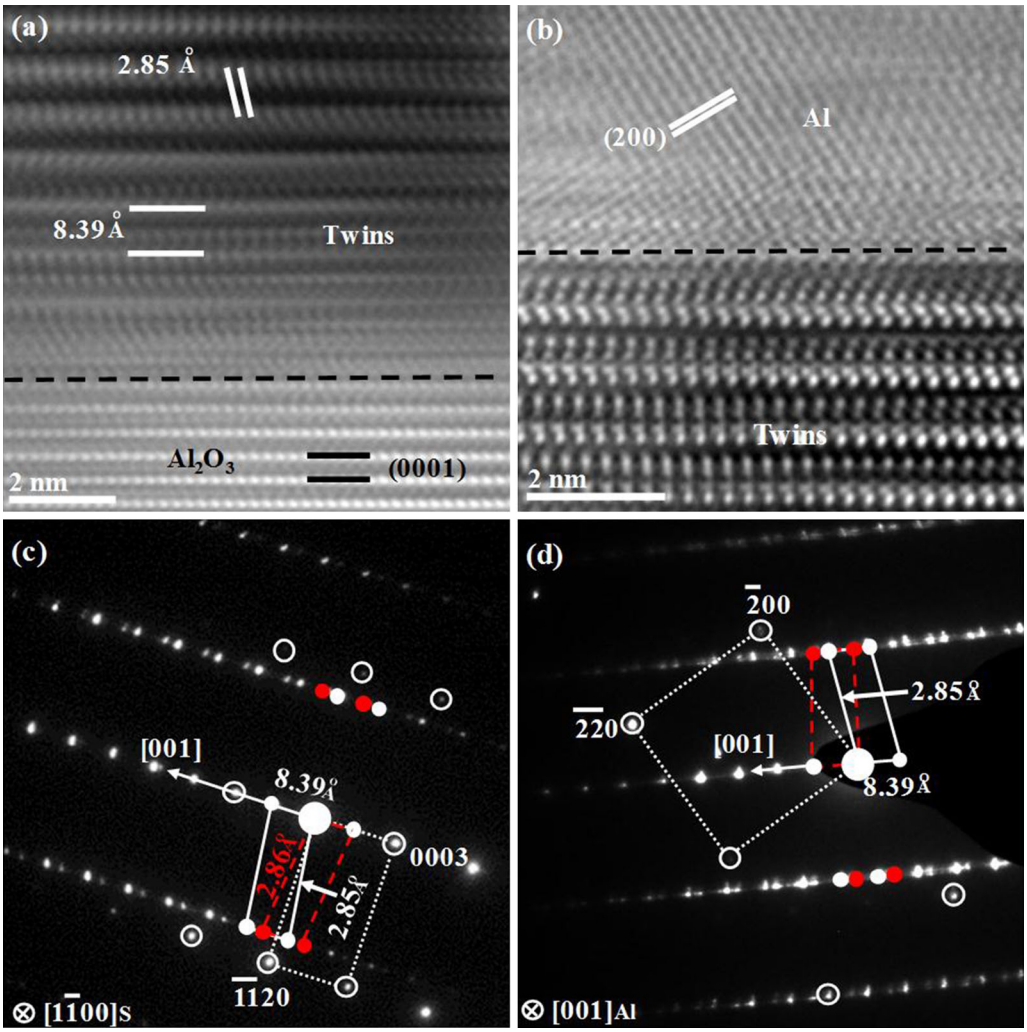

Fig. 5—The cross-sectional HRTEM images of interface between the plate and the Al_2O_3 (0001) substrate with $f = 16.36$ pct taken along Al_2O_3 [1$\bar{1}$00] axis (*a*) and between the Al crystal and the plate viewed from Al [001] axis (*b*). The interface is marked with black dashed line. (*c*) The SADPs on the interface plate/Al_2O_3 show overlapped spots. Among the spots, one set can be identified as Al_2O_3 in [1$\bar{1}$00] zone axis as indexed with large open circles. The other two sets have typical feature of twins with habit plane (100) and invariant direction [001] as schematically illustrated with filled white and red circles in the pattern. (*d*) The SADPs on the interface plate/Al show a set of Al crystal with large open circles and the other two sets are twin as marked with filled white and red circles. The microtwins have the average spacing of plane parallel to interface which is about 0.839 nm and the other spacing along horizontal direction which is 0.285 nm.

3. *Nucleation with coincidence dislocations*

In order to spread dislocations to a poor fit system, coincidence lattice misfit model[39–43] was suggested based upon the matching of multiple lattice planes across the crystal–substrate interface. However, the relationship of interfacial energy and coincidence lattice misfit is absent. Based on the explanation of coincidence in previous studies,[44–47] the total interfacial energy for coincidence lattice misfit is given on some assumptions. Since the coincidence means the periodic extra or missing planes at the interface, the critical thickness h_{cd} to introduce the coincidence dislocations can be calculated according to the critical thickness of edge dislocations,[35] where natural lattice misfit is replaced by coincidence lattice misfit F

$$h_{cd} = \frac{\boldsymbol{b}}{F}\frac{1}{4\pi(1+\nu)}\left(\ln\frac{h_{cd}}{\boldsymbol{b}}+1\right). \qquad [8]$$

The distance of coincidence dislocations is ma_o, so the total length of coincidence dislocations will be $1/ma_o$ per unit area. The coincidence dislocation energy E_{cd} per unit area can be modified as

$$E_{cd} = \frac{G\boldsymbol{b}^2}{4\pi(1-\nu)}\left(\ln\frac{h_{cd}}{\boldsymbol{b}}+1\right)\times\left(\frac{1}{ma_o}\right). \qquad [9]$$

The strain energy E_s per unit area at the interface can be calculated as

$$E_s = 2G\left(\frac{1+\nu}{1-\nu}\right)h_{cd}F^2. \qquad [10]$$

The total interfacial energy, the energy of coincidence dislocation, the strain energy, and the critical thickness

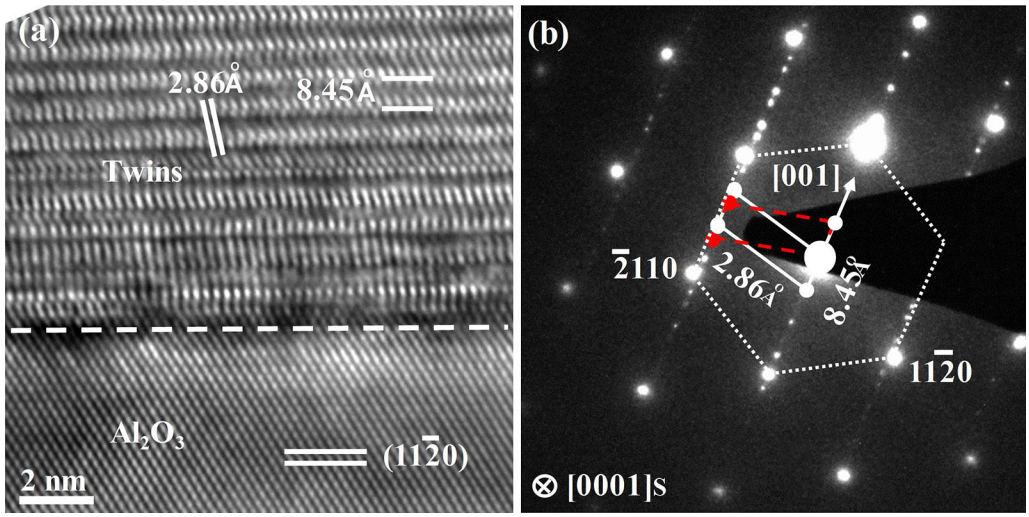

Fig. 6—(*a*) The cross-sectional HRTEM image of interface between plate and Al_2O_3 (11$\bar{2}$0) substrate with $f = 25.03$ pct taken along Al_2O_3 [0001] axis. The interface is marked with white dashed line. (*b*) The SADPs on the interface show overlapped spots. Among the spots, a set can be identified as Al_2O_3 in [0001] zone axis as indexed. The other two sets have typical feature of twins with habit plane (100) and invariant direction [001] as schematically illustrated in the pattern. The microtwins have the average spacing of plane parallel to interface which is about 0.845 nm and the other spacing along horizontal direction which is 0.286 nm.

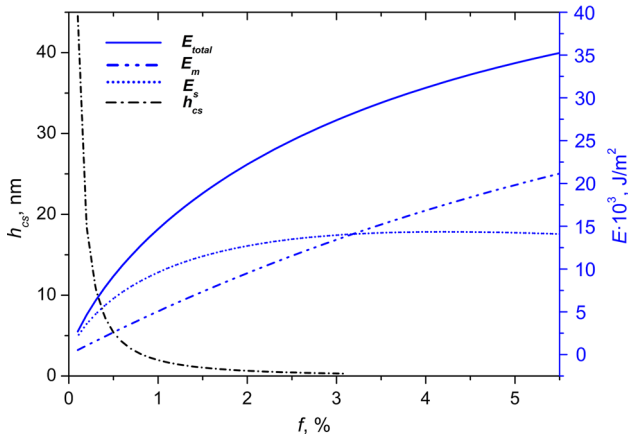

Fig. 7—The calculated total interfacial energy (E_{total}), the mean energy of misfit (E_m), the strain energy (E_s) per unit area, and the critical thickness (h_{cs}) of the homogeneous strain layer as a function of lattice misfit ($f < 3.1$ pct) for nucleation of Al with lattice distortion.

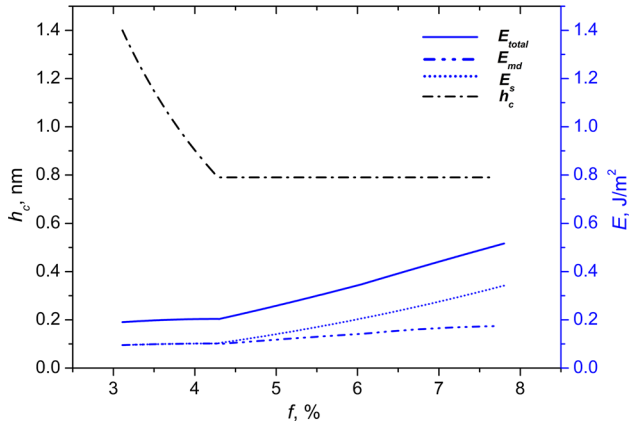

Fig. 8—The calculated total interfacial energy (E_{total}), the energy of dislocation (E_{md}), and the strain energy (E_s) per unit area and critical thickness (h_c) for introducing dislocations as a function of natural lattice misfit ($3.1 < f < 7.8$ pct) for nucleation of Al with natural misfit dislocations.

of coincidence dislocations as a function of corresponding natural lattice misfit can be plotted in Figure 9. For $f = 7.8$ pct, $m(n)$ is about 13, the critical thickness h_{cd} of the coincidence dislocations is 0.49 nm, slightly bigger than critical thickness of a monolayer of Al. If $f = 20.6$ pct, where $m(n) = 5$, the critical thickness is 0.3 nm, about a monolayer thick of Al. Thus, the limitation of the model can be defined within 7.8-20.6 pct. Beyond this range, when a dislocation will be introduced below a thickness of an atomic layer, the model fails.

4. *Nucleation with stacking faults*

From HRTEM results of the system with $f > 13$ pct, the misfit may not be able to be accommodated simply by dislocations and residual strain. Some stacking fault defects like microtwins would be introduced as shown in Figures 5 and 6. The interfacial energy is replaced by the stacking fault energy (E_{SF}) accumulated in the strained area.

$$E_{total} = E_{SF} \quad [11]$$

In our case, the stacking fault energy consists of the twinning energy and other strain energy. It is believed that the twin forms through the change of stacking due to the passage of partial dislocations in *f.c.c.* materials.[48] Therefore for the simplification of calculation, we take the twinning fault energy (E_T) as the stacking fault energy. For multi twin layers, E_{SF} is calculated by

$$E_{SF} = n \cdot E_T, \quad [12]$$

where n is the number of twin layers. The average microtwin layer numbers for Al/Al_2O_3 (0001) and Al/

Al_2O_3 (11$\bar{2}$0) system are about 85 and 76, respectively. Taking the twinning fault energy E_T = 160 mJ/m^2,[49–51] the interfacial energy of Al/Al_2O_3 (0001) and Al/Al_2O_3 (11$\bar{2}$0) per unit area can be given as 13.6 and 12.2 J/m^2.

B. *Experimental Verification on the Models*

1. *Distortion-only nucleation when f < 3.1 pct*

The success of using various substrates to gain high-quality and specially oriented thin film of oxides has opened a new window for the advanced materials fabrication. Tiwari[52] grew epitaxial (100) $NdNiO_3$ films on (100) $SrTiO_3$ substrate with lattice misfit only 2.4 pct. This small lattice misfit makes a cube-on-cube epitaxial growth with limited lattice distortion. The misfit between Al and TiB_2 (Al_3Ti) is also small enough, so that an enhanced heterogeneous nucleation is achieved by adding TiB_2 (Al_3Ti) inoculants.[53] The theoretical upper limit of misfit for distortion-only nucleation is 3.1 pct for Al. Within the misfit range, Al can nucleate on the substrate with limited lattice distortion and the undercooling of Al alloy is less than 1 K (−272 °C), such as the undercooling for nucleation of Al by Al-Ti-B inoculants.[54]

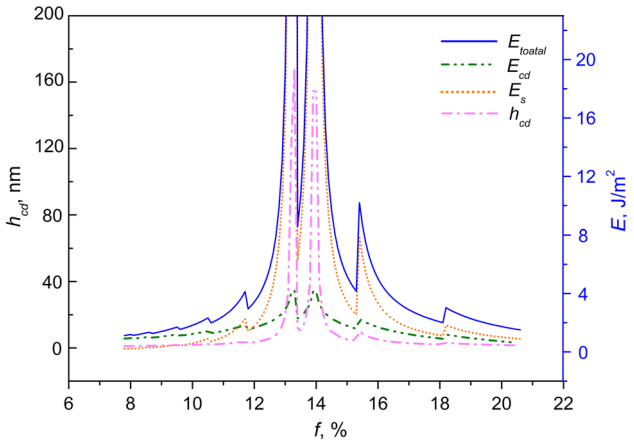

Fig. 9—The calculated total interfacial energy (E_{total}), the energy of coincidence dislocation (E_{cd}), the strain energy (E_s) per unit area, and the critical thickness (h_{cd}) of coincidence dislocations as a function of corresponding natural lattice misfit (f) within the range of 7.8-20.6 pct. The upper limit of corresponding natural lattice misfit is about 20.6 pct as the interfacial energy can be balanced by strain and coincidence dislocations, where $m(n)$ = 5 and the critical thickness of the coincidence dislocations is 0.3 nm, slightly more than a monolayer of Al.

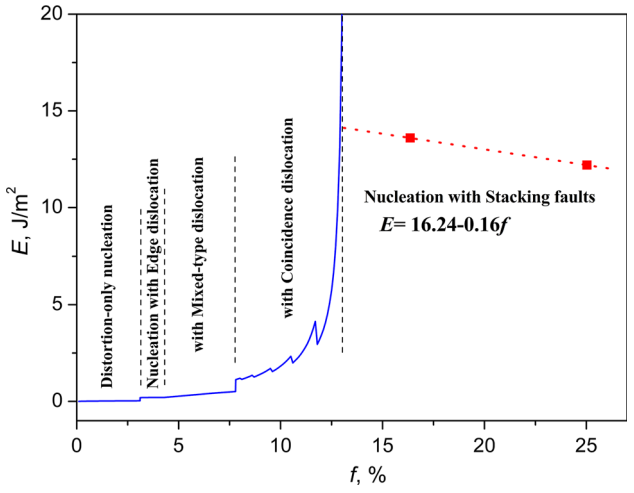

Fig. 10—The total interfacial energy per unit area of various interfaces as a function of natural lattice misfit within the range of 0~25.03 pct, with distortion-only nucleation for small lattice misfit (f < 3.1 pct), nucleation with natural misfit dislocation for misfit range of 3.1-7.8 pct, nucleation with coincidence dislocation for large lattice misfit system (7.8 < f < 13 pct), and stacking faults within the range of 13-25.03 pct.

2. *Nucleation with natural-dislocation when 3.1 < f < 7.8 pct*

An isolated dislocation will be introduced into interface when misfit is over 3.1 pct. Narayan[55] found two kinds of edge dislocation with Burgers vectors of $a/2\langle 101\rangle$ and $a/2\langle 110\rangle$ at GaAs/Si interface when misfit was 4 pct. Lu[38] identified major edge and mixed-type threading dislocations with Burgers vectors of $a/3\langle 11\bar{2}0\rangle$ and $(a+c)/3\langle 11\bar{2}3\rangle$ at GaN/Al_2O_3 interface. These edge and mixed-type dislocations nucleate at the free surface during the growth process and glide to the interface to relax the misfit. The number of edge and mixed-type dislocations is small due to low lattice misfit, for example, there is only one dislocation that can be seen within 0.1 μm length for GaN/Al_2O_3 system.

In our system, Al can nucleate on the substrate with introduced edge and mixed-type dislocations at free surface and its undercooling is only several degrees at the misfit range of 3.1-7.8 pct such as ~3.5 K in (100) Al/(22$\bar{4}$3) Al_2O_3 system. Similarly, the small nucleating undercooling of liquid iron catalyzed by TiN, TiC, and SiC[16] was also found within this misfit range.

3. *Nucleation with coincidence dislocations when 7.8 < f < 13 pct*

The coincidence misfit is based upon matching of integral multiple lattice planes of crystal and substrate. Pant and Zhou[55–57]found the coincidence misfit dislocations at the (11$\bar{2}$0) ZnO/(1$\bar{1}$02) Al_2O_3 interface. The experimental results in this work verified Al nucleates on the substrate by introducing coincidence dislocations when the misfit of the system is located in the range of 7.8 <f < 13 pct. The undercooling is also increased to dozens of degrees, such as in (200) Al/(10$\bar{1}$1) Al_2O_3 system, so does the nucleating undercooling of liquid iron catalyzed by ZrN and WC.[16]

4. *Nucleation with stacking faults as f > 13 pct*

Combining HRTEM observations on Al/Al_2O_3 interface with misfit of 16.36 and 25.03 pct and corresponding interfacial energy analysis, the misfit at this type of interface would be accommodated by stacking fault defects like microtwins and so on. The interfacial energy is replaced by the stacking fault energy accumulated in the strained area when f > 13 pct. According to the detected undercooling within this range, a linear relationship between the interfacial energy and lattice misfit was assumed as follows

$$E = a \cdot f + b. \quad [13]$$

Given, f = 16.36 pct, Al/Al_2O_3 (0001) system, total energy is 13.6 J/m^2 and f = 25.03 pct, Al/Al_2O_3 ($11\bar{2}0$) system, total energy is 12.2 J/m^2. The factors of Eq. [13] can be fixed as $a = -0.16$, $b = 16.24$. Based on this assumption, the average thickness of the stacking fault layer should have linear relationship with lattice misfit as well. There is an indirect evidence that only one layer microtwins were confirmed at the interface of Al (111) film and Al_2O_3 (0001) substrate by depositing method,[58] where the lattice misfit is 6.08 pct. But due to the fabrication method difference, the lattice misfit limitation for introducing stacking fault may move forward.

5. *Integrated interfacial energy model through the range of $f < 25.03$ pct*

The total interfacial energy per unit area of various interfaces as a function of natural lattice misfit within the predictable range of 0-25.03 pct of Al/Al_2O_3 system is shown in Figure 10, calculated through van der Mere model ($f < 3.1$ pct), modified NLM model for misfit range of 3.1-7.8 pct, coincidence model for large lattice misfit system ($7.8 < f < 13$ pct), and stacking fault model within the range of 13-25.03 pct, respectively.

C. *Predictable Heterogeneous Undercooling Using Integrated Model*

According to the CNT, the undercooling for nucleation ΔT_c is simply related by

$$\Delta T_c = \frac{2\sigma_{LS} T_m}{\Delta H_V \times r} \cong \frac{2\sigma_{LS}}{\Delta S_V \times r} \quad [14]$$

where σ_{LS} is the solid–liquid interfacial energy per unit area, T_m is the melting point of metal, ΔH_V is the enthalpy change, ΔS_V is the entropy of fusion per unit volume, taking an available value[59] $\Delta S_V = 1.112 \times 10^6$ J/K $mo1^3$, r is the particle radius and usually at the range of 0.1-10μm, setting the value as the average radius of the Al crystals on the interface, $r = 1\mu$m here. Replacing σ_{LS} with the above calculated interfacial energy E_{total}, the undercooling of Al as a function of lattice misfit can be predicted for $f < 13$ pct, as shown in Figure 11 left. For $f > 13$ pct, the interfacial energy can be replaced by stacking fault energy as predicted in Eq. [13]. Thus, a linear relationship between undercooling and lattice misfit can be obtained under the newly developed stacking fault model, as shown in Figure 11 right.

The undercooling of Al nucleated on various Al_2O_3 substrates in our experiment were plotted in the figure along with the data obtained from liquid Al nucleated by Al-Ti-B inoculants[54] and liquid iron catalyzed by different carbide and nitride additions.[16] It shows that the predicted undercooling with the modified existing misfit-interfacial energy models agrees with experimental results very well even when $f > \sim 13$ pct where stacking fault energy dominates the interfacial energy for nucleation.

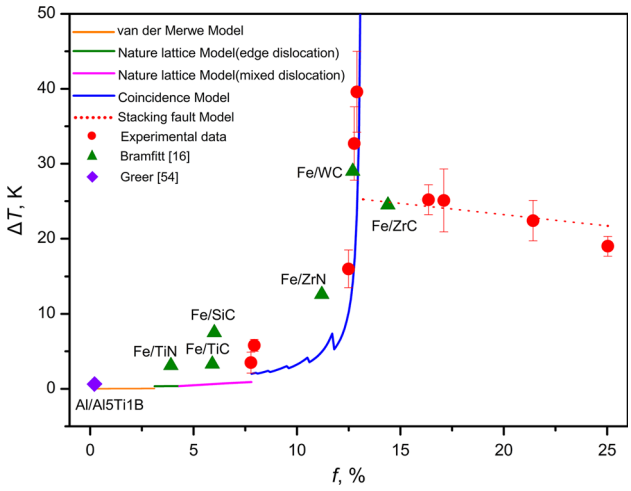

Fig. 11—The relationship between the predicted and experimental undercooling as a function of lattice misfit. The experimental undercoolings include the data of Al nucleated on various Al_2O_3 substrates in our experiment and other data for liquid Al nucleated by Al-Ti-B inoculants[54] and liquid iron catalyzed by different carbide and nitride additions.[16] The predicted undercooling with the modified existing misfit-interfacial energy models agrees with experimental results very well when $f < \sim 13$ pct and a linear relationship between undercooling and lattice misfit presents beyond 13 pct under newly developed stacking fault model.

V. CONCLUSIONS

The available experimental evidence obtained in Al/Al_2O_3 systems in the present work indicates that the lattice structure of nucleation substrate does affect the nucleation behavior of new crystals. A series of lattice misfits were obtained by nucleating Al on different termination planes of single-crystal alumina substrates. The undercooling of the nucleating system can be predicted through integrated misfit-interfacial energy models. Within small lattice misfit ($f < 3.1$ pct), the nucleated phase fits the substrate with limited lattice distortion which follows van der Mere model. With the increase of lattice misfit, the edge dislocations or mixed-type dislocations are introduced and a modified NLM model was proposed for misfit range of 3.1-7.8 pct. In a large lattice misfit system ($7.8 < f < 13$ pct), the misfit is accommodated by strain and coincidence dislocations according to coincidence misfit model. Stacking fault model involving misfit-interfacial energy was developed for lattice misfit beyond 13 pct, where the misfit is accommodated by some stacking fault defects like microtwins and the interfacial energy is replaced by stacking fault energy such as twinning energy. Thus, a general misfit-interfacial energy model for heterogeneous nucleation interface is developed in this work within an extended misfit range ($f < 25.03$ pct). HRTEM analysis indicates that the singularity of undercooling *vs* misfit plot is due to the existence of an intermediate heavily twined plate (Al phase) when lattice misfit is larger than 13 pct.

ACKNOWLEDGMENTS

The authors are grateful for the financial support from NSFC (No. 51174134, No. 51474148), Shanghai STC (No. 11JC1405900), and NBRPC (No. 2011CB012900).

REFERENCES

1. K.F. Kelton and A.L. Greer: *Nucleation in Condensed Matter*, Pergamon, Oxford, 2010, pp. 19–28.
2. B. Cantor: *Phil. Trans. R. Soc. Lond. A*, 2003, vol. 361, pp. 409–17.
3. O.M. Magnussen, B.M. Ocko, M.J. Regan, K. Penanen, P.S. Pershan, and M. Deutsch: *Phys. Rev. Lett.*, 1995, vol. 74 (22), pp. 4444–47.
4. S.H. Oh, Y. Kauffmann, C. Scheu, W.D. Kaplan, and M. Rühle: *Science*, 2005, vol. 310 (5748), pp. 661–63.
5. S.B. Lee and Y.M. Kim: *Acta Mater.*, 2011, vol. 59, pp. 1383–388.
6. M. Gandman, Y. Kauffmann, C.T. Koch, and W.D. Kaplan: *Phys. Rev. Lett.*, 2013, vol. 110 (8), p. 086106.
7. L. Yang, C.E. Birchenall, G.M. Pound, and M.T. Simnad: *Acta Metall.*, 1954, vol. 2 (3), pp. 462–69.
8. M. Qian: *Acta Mater.*, 2007, vol. 55, pp. 943–53.
9. M. Qian and J. Ma: *J Cryst. Growth.*, 2012, vol. 355 (1), pp. 73–77.
10. D. Turnbull and B. Vonnegut: *Ind. Eng. Chem.*, 1952, vol. 44 (6), pp. 1292–98.
11. F.C. Frank and J.H. van der Merwe: *Proc. R. Soc. A*, 1053, vol. 1949 (198), pp. 205–16.
12. J.W. Matthews and A.E. Blakeslee: *J. Cryst. Growth*, 1974, vol. 27, pp. 118–25.
13. R. People and J.C. Bean: *Appl. Phys. Lett.*, 1985, vol. 47 (3), pp. 322–24.
14. N.H. Fletcher and K.W. Lodge: *Epitaxial Growth, Part B*, Academic Press, New York, J. W. Matthews, 1975, pp. 529–30.
15. R.W. Vook and C.T. Horng: *Philos. Mag.*, 1976, vol. 33 (5), pp. 843–61.
16. B.L. Bramfitt: *Metall. Trans.*, 1970, vol. 1 (7), pp. 1987–995.
17. M. Zarif, B. McKay, J. Li, and P. Schumacher: *BHM.*, 2010, vol. 155 (11), pp. 506–11.
18. M. Zarif, B. Mckay, and P. Schumacher: *Metall. Mater. Trans. A*, 2011, vol. 42A (6), pp. 1684–91.
19. L. Yang, M. Xia, and J.G. Li: *Mater. Lett.*, 2014, vol. 132, pp. 52–54.
20. P.M. Kelly and M.-X. Zhang: *Metall. Mater. Trans. A*, 2006, vol. 37A, pp. 833–39.
21. G.J. Shiflet and J.H. Van der Merwer: *J. Electron. Mater.*, 1991, vol. 20, pp. 785–91.
22. M.-X. Zhang and P.M. Kelly: *Acta Mater.*, 2005, vol. 53 (4), pp. 1073–84.
23. M.-X. Zhang and P.M. Kelly: *Acta Mater.*, 2005, vol. 53 (4), pp. 1085–96.
24. M.-X. Zhang, S.Q. Chen, H.-P. Ren, and P.M. Kelly: *Metall. Mater. Trans. A*, 2008, vol. 39A, pp. 1077–86.
25. M.-X. Zhang, D. Qiu, and P.M. Kelly: *Thin Solid Films*, 2008, vol. 516, pp. 5498–5502.
26. R. Feder and A.S. Nowick: *Phys. Rev.*, 1958, vol. 109 (6), pp. 1959–63.
27. W.M. Yim and R.J. Paff: *J. Appl. Phys.*, 1974, vol. 45 (3), pp. 1456–57.
28. Y. Wang, H.T. Li, and Z. Fan: *Trans. Indian Inst. Met.*, 2012, vol. 65 (6), pp. 653–61.
29. A.M. Pérez-Sierra, J. Pons, R. Santamarta, P. Vermaut, and P. Ochin: *Acta Mater.*, 2015, vol. 93, pp. 164–74.
30. J.H. van der Merwe: *J. Appl. Phys.*, 1963, vol. 34 (1), pp. 117–22.
31. R. Peierls: *Proc. Phys. Soc.*, 1940, vol. 52 (1), pp. 34–37.
32. F.R.N. Nabarro: *Proc. Phys. Soc.*, 1947, vol. 59 (2), pp. 256–72.
33. J.H. van der Merwe: *J. Appl. Phys.*, 1963, vol. 34 (1), pp. 123–27.
34. Z. Fan: *Metall. Mater. Trans. A*, 2013, vol. 44A (3), pp. 1409–18.
35. W.A. Jesser and J.W. Matthews: *Philos. Mag.*, 1967, vol. 15 (138), pp. 1097–1106.
36. J.W. Matthews and A.E. Blakeslee: *J. Cryst. Growth*, 1975, vol. 29, pp. 273–80.
37. K. Shiojima: J. *Vac. Sci. Technol. B,* 2000, vol. 18, no. 1, pp. 37–40.
38. L. Lu, Z.Y. Gao, B. Shen, F.J. Xu, S. Huang, Z.L. Miao, Y. Hao, Z.J. Yang, G.Y. Zhang, X.P. Zhang, J. Xu, and D.P. Yu: *J. Appl. Phys.*, 2008, vol. 104, p. 123525.
39. M.J. Weins, H. Gleiter, and B. Chalmers: *J. Appl. Phys.*, 1971, vol. 42 (7), pp. 2639–45.
40. R.W. Balluffi, Y. Komem, and T. Schober: *Surf. Sci.*, 1972, vol. 31, pp. 68–103.
41. R.W. Vook: *Thin Solid Films*, 1979, vol. 64, pp. 91–102.
42. R.W. Vook: *Int. Met. Rev.*, 1982, vol. 27 (4), pp. 209–45.
43. D. Cherns and C.J. Kiely: *Mater. Sci. Eng., A*, 1989, vol. 113, pp. 43–50.
44. A. Trampert and K.H. Ploog: *Cryst. Res. Technol.*, 2000, vol. 35 (6-7), pp. 793–806.
45. K.H.L. Zhang, V.K. Lazarov, P.L. Galindo, F.E. Oropeza, D.J. Payne, H.H.-C. Lai, and R.G. Egdell: *Cryst. Growth Des.*, 2012, vol. 12 (2), pp. 1000–07.
46. N.H. Fletcher: *J. Appl. Phys.*, 1964, vol. 35 (1), pp. 234–40.
47. N.H. Fletcher: *Philos. Mag.*, 1967, vol. 16 (139), pp. 159–64.
48. S. Kibey, J.B. Liu, D.D. Johnson, and H. Sehitoglu: *Acta Mater.*, 2007, vol. 55 (20), pp. 6843–51.
49. J.P. Hirth and J. Lothe: *Theory of dislocations*, 2nd ed., Malabar, Krieger Pub. Co, 1982, p. 839.
50. M.I. Baskes: *Phys. Rev. B*, 1992, vol. 46 (5), pp. 2727–42.
51. S. Ogata, J. Li, and S. Yip: *Sci.*, 2002, vol. 298 (25), pp. 807–11.
52. A. Tiwari, J. Narayan, C. Jin, and A. Kvit: *Appl. Phys. Lett.*, 2002, vol. 80 (8), pp. 1337–39.
53. Z. Fan, Y. Wang, Y. Zhang, T. Qin, X.R. Zhou, G.E. Thompson, T. Pennycook, and T. Hashimoto: *Acta Mater.*, 2015, vol. 84, pp. 292–304.
54. A.L. Greer, A.M. Bunn, A. Tronche, P.V. Evans, and D.J. Bristow: *Acta Mater.*, 2000, vol. 48, pp. 2823–35.
55. J. Narayan: *Acta Mater.*, 2013, vol. 61, pp. 2703–24.
56. P. Pant, J.D. Budai, and J. Narayan: *Acta Mater.*, 2010, vol. 58, pp. 1097–1103.
57. H. Zhou, M.F. Chisholm, P. Pant, H.J. Chang, J. Gazquez, S.J. Pennycook, and J Narayan: *Appl. Phys. Lett.*, 2010, vol. 97 (12), p. 121914.
58. D.L. Medlin, K.F. McCarty, R.Q. Hwang, S.E. Guthrie, and M.I. Baskes: *Thin Solid Films*, 1997, vol. 299 (1-2), pp. 110–14.
59. W.F. Gale, and T.C. Totemeier: Smithells metals reference book, 8th ed., in ed. E. A. Brandes, *Thermochemical data*, Butterworths, London, 1983, pp. 8-1–14-1.